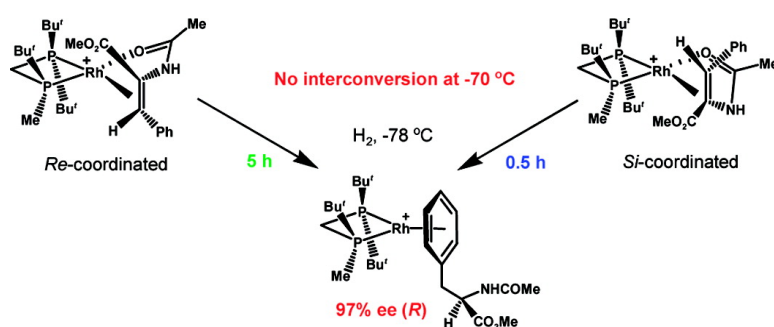Article

Asymmetric Hydrogenation Catalyzed by a Rhodium Complex of (*R*)-(*tert*-Butylmethylphosphino)(di-*tert*-butylphosphino)methane: Scope of Enantioselectivity and Mechanistic Study

Ilya D. Gridnev, Tsuneo Imamoto, Garrett Hoge, Mitsuhiro Kouchi, and Hidetoshi Takahashi

More About This Article

Additional resources and features associated with this article are available within the HTML version:

- Supporting Information
- Links to the 6 articles that cite this article, as of the time of this article download
- Access to high resolution figures
- Links to articles and content related to this article
- Copyright permission to reproduce figures and/or text from this article

View the Full Text HTML

Asymmetric Hydrogenation Catalyzed by a Rhodium Complex of (R)-(tert-Butylmethylphosphino)(di-tert-butylphosphino)-methane: Scope of Enantioselectivity and Mechanistic Study

Ilya D. Gridnev,*,†,‡ Tsuneo Imamoto,*,§ Garrett Hoge,*,‖ Mitsuhiro Kouchi,‡ and Hidetoshi Takahashi§

Graduate School of Science and Engineering, Tokyo Institute of Technology, 2-12-1 Ookayama, Meguro-ku, Tokyo 152-8552, Japan, Department of Chemistry, Graduate School of Science, Tohoku University, Sendai 980-8578, Japan, Department of Chemistry, Graduate School of Science, Chiba University, Chiba 263-8522, Japan, and High Pressure Laboratory, Chemical R&D, Pfizer Global R&D, 2800 Plymouth Road, Ann Arbor, Michigan 48105

Received August 30, 2007; E-mail: gridnev.i.aa@m.titech.ac.jp

Abstract: The rhodium complex of (R)-(tert-butylmethylphosphino)(di-tert-butylphosphino)methane used in Rh-catalyzed asymmetric hydrogenation of representative substrates **3**−**14** demonstrated high catalytic activity coupled with wide scope and nearly perfect enantioselectivity. Mechanistic studies (NMR and DFT computations) were carried out in order to investigate the mechanism of the enantioselection in the asymmetric hydrogenation of (Z)-α-acetamidocinnamate (**3**). Although catalyst−substrate complexes **15a,b** with the double bond coordinated near the non-"chiral" phosphorus atom were formed as kinetic products upon the addition of **3** to solvate complex **2** at −100 °C, they rapidly rearranged to more stable isomers **15c,d** with the double bond coordinated near the "chiral" phosphorus atom. The thermodynamic and kinetic parameters of the interconversion between **15c** and **15d** were determined by NMR; mainly, the interconversion occurred intramolecularly via nonchelating catalyst−substrate complexes **16**. The equilibrium between **15d** and **16d** was directly observed from NMR line shape changes at temperatures ranging from −100 to −40 °C, whereas no such equilibrium was observed for **15c**. This result was accounted for computationally by determining the corresponding transition states for the methanol insertion into **15c,d**. Three sets of experiments of the low-temperature hydrogenation of different catalyst−substrate complexes gave the same order and sense of enantioselectivity (97% ee (R)) even in the case when **15c**, having Re-coordinated double bond, was hydrogenated under the conditions precluding its isomerization to **15d**. It was concluded that the hydrogenation of **15c,d** does not occur directly, but is preceded by the dissociation of the double bond to result in the more reactive species **16**. This indicates that enantioselection must occur at a later step of the catalytic cycle. DFT computations of association and migratory insertion steps suggest that enantioselection takes place during the association step when chelating dihydride **19d·**MeOH is formed from nonchelating dihydride **18d**.

1. Introduction

The mechanism of Rh-catalyzed asymmetric hydrogenation has been in the focus of active academic research in the past three decades.[1−12] This mechanistic investigation is fueled both by the practical importance of the reaction itself and by the abundance of experimental data. Much effort has been dedicated to intercepting and characterizing reaction intermediates during the process of asymmetric hydrogenation. This concentration on asymmetric hydrogenation is unrivaled by mechanistic investigations of other catalytic processes.[13−15] Moreover, large-scale *ab initio* computations that describe detailed reaction pathways of the catalytic cycle are now available.[16−20]

† Tokyo Institute of Technology.
‡ Tohoku University.
§ Chiba University.
‖ Pfizer Global R&D.

(1) Knowles, W. S. Asymmetric Hydrogenations (Nobel Lecture). *Angew. Chem., Int. Ed.* **2002**, *41*, 1998.
(2) Noyori, R. Asymmetric Catalysis: Science and Opportunities (Nobel Lecture). *Angew. Chem., Int. Ed.* **2002**, *41*, 2008.
(3) Noyori, R. A*symmetric Catalysis in Organic Synthesis*; John Wiley & Sons: New York, 1994; pp 16−94.
(4) Ohkuma T.; Kitamura M.; Noyori R. In *Catalytic Asymmetric Synthesis*; Ojima, I., Ed.; Wiley-VCH: Weinheim, 2000; pp 1−110.
(5) Brown, J. M. In *Comprehensive Asymmetric Catalysis*; Jacobsen, E. N., Pfaltz, A., Yamamoto, H., Eds.; Springer: Berlin, 1999; Vol. 1, pp 119−182.
(6) Crepy, K. V. L.; Imamoto, T. *Adv. Synth. Catal.* **2003**, *345*, 79.
(7) Gridnev, I. D.; Imamoto, T. *Acc. Chem. Res.* **2004**, *37*, 633.
(8) Kagan, H. B.; Langois, N.; Dang, T. P. *J. Organomet. Chem.* **1975**, *90*, 353.
(9) Schrock, R. R.; Osborn, J. A. *J. Am. Chem. Soc.* **1976**, *98*, 134.
(10) Halpern, J.; Riley, D. P.; Chan, A. S. C.; Pluth, J. J. *J. Am. Chem. Soc.* **1977**, *99*, 8055.
(11) Brown, J. M.; Chaloner, P. A. *J. Chem. Soc., Chem. Commun.* **1978**, 321.
(12) Chan, A. S. C; Halpern, J. *J. Am. Chem. Soc.* **1980**, *102*, 838.
(13) Gridnev, I. D.; Higashi, N.; Asakura, K.; Imamoto, T. *J. Am. Chem. Soc.* **2000**, *122*, 7183.
(14) Giernoth, R.; Heinrich, H.; Adams, N.; Deeth, R. J.; Bargon, J.; Brown, J. M. *J. Am. Chem. Soc.* **2000**, *122*, 12381.
(15) Imamoto, T.; Yashio, K.; Crépy, K. V. L.; Katagiri, K.; Takahashi, H.; Kouchi, M.; Gridnev, I. D. *Organometallics* **2006**, *25*, 908.
(16) (a) Landis, C. R.; Feldgus, S. *Angew. Chem., Int. Ed.* **2000**, *39*, 2863. (b) Feldgus, S.; Landis, C. R. *J. Am. Chem. Soc.* **2000**, *122*, 12714.

Scheme 1. Mechanism of Asymmetric Hydrogenation Implying the Chelate Coordination of the Substrate Prior to the Oxidative Addition of Dihydrogen
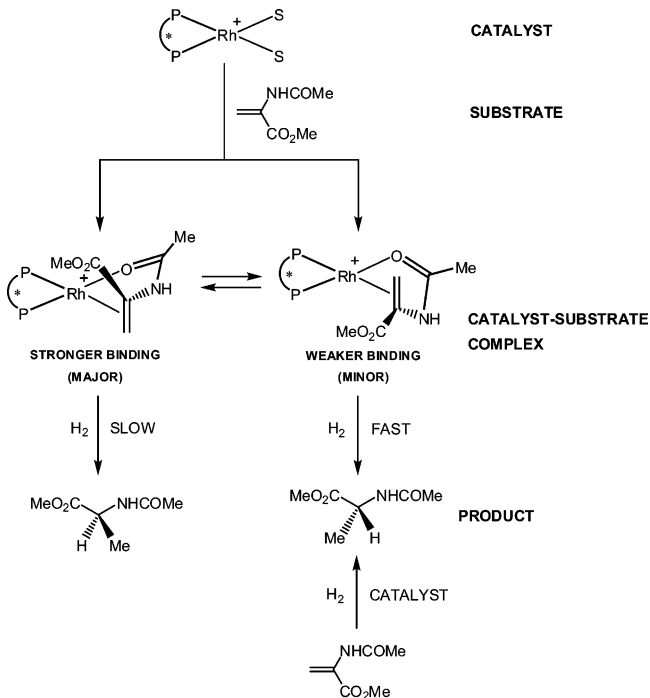

The most important conclusion that can be derived from these extensive mechanistic studies is a clear understanding of the intrinsic mechanism of enantioselection. This knowledge is important for design of chiral catalysts and the optimization of reaction conditions. It has been widely accepted initially that the stereoselection in Rh-catalyzed asymmetric hydrogenation takes place via the difference in reactivity of diastereomeric square planar catalyst−substrate complexes toward dihydrogen. This conclusion originated from the early experiments of Brown[21] and Halpern,[22−24] in which the structures of the relatively reactive diastereomers of the catalyst−substrate complexes have been in accord with the sense of enantioselection observed in these reactions (Scheme 1). Landis and Halpern have studied the kinetics of measurable reaction steps and equilibria for the case of asymmetric hydrogenation of methyl (Z)-α-acetamidocinnamate catalyzed by Rh−DIPAMP, and showed that they are in qualitative agreement with the expected patterns.[25]

However, further research has demonstrated a considerable diversification of the mechanistic details. Thus, a very late agostic intermediate has been shown to be involved in a reversible equilibrium with the catalyst in case of asymmetric hydrogenation with the Rh−PHANEPHOS complex.[26] Moreover, it has been shown that enantioselectivities comparable to

those obtained in the catalytic reactions can be obtained by the low-temperature reactions of solvate dihydrides derived from the Rh complexes of electron-rich diphosphines with representative substrates.[27] These observations opened the doors for the possibility of the hydrogen activation prior to the substrate coordination in these reactions.[7] Hence, according to the recent point of view, the mechanism of enantioselection can be depending on the exact combination of the ligand and the substrate.

The more reactive diastereomer of the catalyst−substrate complex in early mechanistic experiments was less abundant in the equilibrium mixture (MINOR in Scheme 1). That experimental observation positioned the enantioselective Rh-catalyzed hydrogenation apart from enzymatic reactions that are believed to apply structural "Lock-and-Key" recognition between the substrate and the enzyme.[28] However, in view of the recent research, it became clear that there is no evident cause-and-effect relationship between the selectivity of substrate binding by the catalyst and the relative reactivity of the resulting catalyst−substrate complexes toward hydrogen. Landis et al. showed computationally how the definite asymmetric environment of the Rh atom can result simultaneously in decreasing stability and increasing reactivity toward dihydrogen in the catalyst−substrate complex of DuPHOS−Rh with α-formami-doacrylonitrile.[16] So far, however, there is no reason to believe that this type of structure−reactivity correlation should be the same for all other catalyst−substrate combinations. Evans et al. reported a P/S ligand whose Rh chelate produced a single isomer of the catalyst−substrate complex with the double bond coordinated accordingly to the observed sense of induction.[29] Similar observations were later reported by Heller et al. for the DIPAMP complexes of β-acylaminoacrylates.[30] Hence, the real understanding of the correlation between the structure of a catalyst−substrate complex and its reactivity toward hydrogen has not been achieved so far.
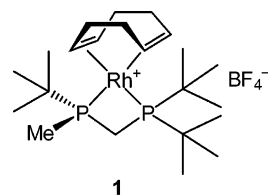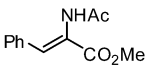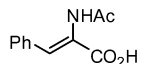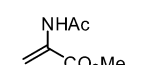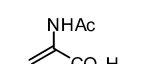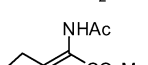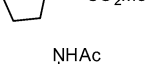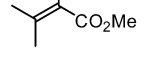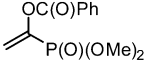

Structure of complex **1**

In this work, we investigated in detail the mechanism of asymmetric hydrogenation catalyzed by a Rh-complex of (R)-(*tert*-butylmethylphosphino)(di-*tert*-butylphosphino)methane

(17) Feldgus, S.; Landis, C. R. *Organometallics* **2001**, *20*, 2374.
(18) Li, M.; Tang, D.; Luo, X.; Shen, W. *Int. J. Quant. Chem.* **2005**, *102*, 53.
(19) Mori, S.; Vreven, T.; Morokuma, K. *Chem. Asian J.* **2006**, *1*, 391.
(20) Donoghue, P. J.; Helquist, P.; Wiest, O. *J. Org. Chem.* **2007**, *72*, 839.
(21) Brown, J. M.; Chaloner, P. A. *J. Chem. Soc., Chem. Commun.* **1980**, 344.
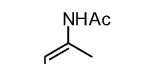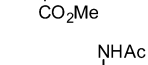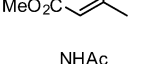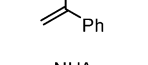(22) Chua, P. S.; Roberts, N. K.; Bosnich, B.; Okrainski, S. J.; Halpern, J. *J. Chem. Soc., Chem. Commun.* **1981**, 1278.
(23) Halpern, J. *Science* **1982**, *217*, 401.
(24) Halpern, J. *Asymmetric Catalytic Hydrogenation: Mechanism and Origin of Enantioselection* in *Asymmetric Synthesis*; Morrison, J. D., Ed.; Academic Press: Orlando, 1985; Vol. 5, pp 41−69.
(25) Landis, C. R.; Halpern, J. *J. Am. Chem. Soc.* **1987**, *109*, 1746.
(26) Heinrich, H.; Giernoth, R.; Bargon, J.; Brown, J. M. *Chem. Commun.* **2001**, 1296.
(27) (a) Gridnev, I. D.; Higashi, N.; Asakura, K.; Imamoto, T. *J. Am. Chem. Soc.* **2000**, *122*, 7183. (b) Gridnev, I. D.; Higashi, N.; Imamoto, T. *J. Am. Chem. Soc.* **2000**, *122*, 10486. (c) Gridnev, I. D.; Yasutake, M.; Higashi, N.; Imamoto, T. *J. Am. Chem. Soc.* **2001**, *123*, 5268. (d) Gridnev, I. D.; Higashi, N.; Imamoto, T. *J. Am. Chem. Soc.* **2001**, *123*, 4631. (e) Gridnev, I. D.; Yamanoi, Y.; Higashi, N.; Tsuruta, H.; Yasutake, M.; Imamoto, T. *Adv. Synth. Catal.* **2001**, *343*, 118. (f) Gridnev, I. D.; Higashi, N.; Imamoto, T. *Organometallics* **2001**, *20*, 4542. (g) Yasutake, M.; Gridnev, I. D.; Higashi, N.; Imamoto, T. *Org. Lett.* **2001**, *3*, 1701. (h) Gridnev, I. D.; Yasutake, M.; Imamoto, T.; Beletskaya, I. P. *Proc. Natl. Acad. Sci. U.S.A.* **2004**, *101*, 5385.
(28) Fischer, E. *Ber. Dtsch. Chem. Ges.* **1894**, *27*, 2985.
(29) Evans, D. A.; Michael, F. E.; Tedrow, J. S.; Campos, K. R. *J. Am. Chem. Soc.* **2003**, *125*, 3534.
(30) (a) Drexler, H.-J.; Baumann, W.; Schmidt, T.; Zhang, S.; Sun, A.; Spannenberg, A.; Fischer, C.; Buschmann, H.; Heller, D. *Angew. Chem., Int. Ed.* **2005**, *44*, 1184. (b) Schmidt, T.; Baumann, W.; Drexler, H.-J.; Arrieta, A.; Heller, D.; Buschmann, H. *Organometallics* **2005**, *24*, 3842.

Table 1. Asymmetric Hydrogenation of Prochiral Substrates Catalyzed by Rh Complex **1**
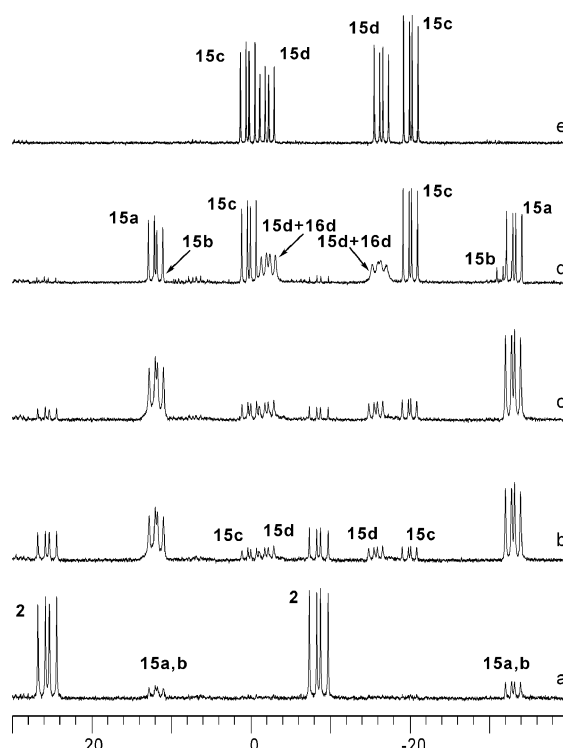
$$\text{Substrate} \xrightarrow[\text{MeOH, rt}]{\text{H}_2, \text{ cat (s/c = 100)}} \text{Product}$$

substrate		H₂ pressure (atm)	time (h)	ee (%) of product
Ph⟍=⟍NHAc CO₂Me	(3)	3	0.1	>99 (R)
Ph⟍=⟍NHAc CO₂H	(4)	3	0.1	>99 (R)
NHAc CO₂Me	(5)	3	0.1	>99 (R)
NHAc CO₂H	(6)	3	0.1	>99 (R)
cyclopentylidene NHAc CO₂Me	(7)	3	0.1	>99 (R)
NHAc CO₂Me	(8)	2	1	98 (R)
OC(O)Ph P(O)(OMe)₂	(9)	3	2	99 (R)
NHAc CO₂Me	(10)	1	0.25	99 (R)
MeO₂C NHAc	(11)	1	0.25	96 (R)
NHAc Ph	(12)	2	1	98 (R)
NHAc Bu-t	(13)	3	2	99 (S)
CO₂Me CO₂Me	(14)	2	1	98 (S)

(**1**).[31,32] Using the results of extensive NMR investigations and computational analysis of real systems, we present an explanation for the different reactivities of diastereomeric catalyst–substrate complexes as well as a new approach to rationalize the enantioselection in Rh-catalyzed asymmetric hydrogenation.

2. Results and Discussion

2.1. Scope of Asymmetric Hydrogenation Catalyzed by Rh Complex 1. The scope of asymmetric hydrogenation catalyzed by complex **1** is shown in Table 1.

Analyzing the data of Table 1, one can conclude that Rh complex **1** is a versatile catalyst: it gives almost perfect stereoselectivity when hydrogenating dehydroamino acids **4** and **6**, and their esters **3** and **5**, including β,β-disubstituted compounds **7** and **8** which are usually very difficult substrates for asymmetric hydrogenation. Other classes of prochiral com-

(31) Hoge, G.; Wu, H.-P.; Kissel, W. S.; Pflum, D. A.; Greene, D. J.; Bao, J. *J. Am. Chem. Soc.* **2004**, *126*, 5966.
(32) Hoge, G.; Wu, H.-P. *Org. Lett.* **2004**, *6*, 3645.

Figure 1. Evolution of the ³¹P spectrum of the sample obtaned by adding 1.5 equiv of MAC **3** to a sample containing the solution of the solvate complex **2** precooled to −100 °C: a) immediately after addition; b) after 30 min at −100 °C; c) after 1 h at −100 °C; d) the temperature raised to −80 °C and the spectrum taken immediately (the still broadened left multiplet of **15b** is under the much more intensive signal of **15a**; signals of **15d** are broad due to the fast equilibrium with **16d**, see Figure 5 and further discussion); e) the temperature raised to −40 °C and the spectrum taken immediately.

pounds, such as phosphonate **9**, β-dehydroamino acids **10** and **11**, enamides **12** and **13**, and itaconic ester **14**, can be also hydrogenated using **1** as a catalyst precursor with very high ee's. The very similar performance of (E)- and (Z)-β-dehydroamino acids enables use of isomeric mixtures as substrates. The opposite sense of enantioselection for phenyl (**12**)- and *tert*-butyl (**13**)-substituted enamides is in accord with previous observations made for other Rh complexes of chiral diphosphines as catalysts.

2.2. Catalytic Cycle in the Asymmetric Hydrogenation of Methyl (Z)-α-Acetamidocinnamate. 2.2.1. Reaction of Solvate Complex 2 with Methyl (Z)-α-Acetamidocinnamate (3). Hydrogenation of catalytic precursor **1** at ambient temperature for 1.5 h yielded the corresponding solvate complex **2**. We investigated the formation of catalyst–substrate complexes by mixing solutions of **2** and MAC (**3**, 1.5-fold excess) at −100 °C and putting the resulting reaction mixture in the probe of an NMR spectrometer precooled to the same temperature. The changes observed in the ³¹P NMR spectrum of the thus-prepared sample are shown in Figure 1. First, two kinetic products are formed (**15a,b**, Scheme 2). The signals of **15a,b** in the ³¹P NMR spectrum at −100 °C are notably broader than the signals of **2** at the same temperature (Figure 1a). At −80 °C, the signals of **15a,b** became sharp, enabling the integration; the ratio **15a**:**15b** was 5:1 (Figure 1d). These line shape changes indicate that both **15a** and **15b** are involved in some equilibria that are fast at −80 °C and become slow in the NMR time scale at −100 °C. Unfortunately, the irreversible rearrangement of **15a,b** to

Scheme 2. Reaction of Solvate Complex **2** with MAC **3**. Red Numbers Indicate the Relative Energies Computed on the B3LYP/SDD Level of Theory
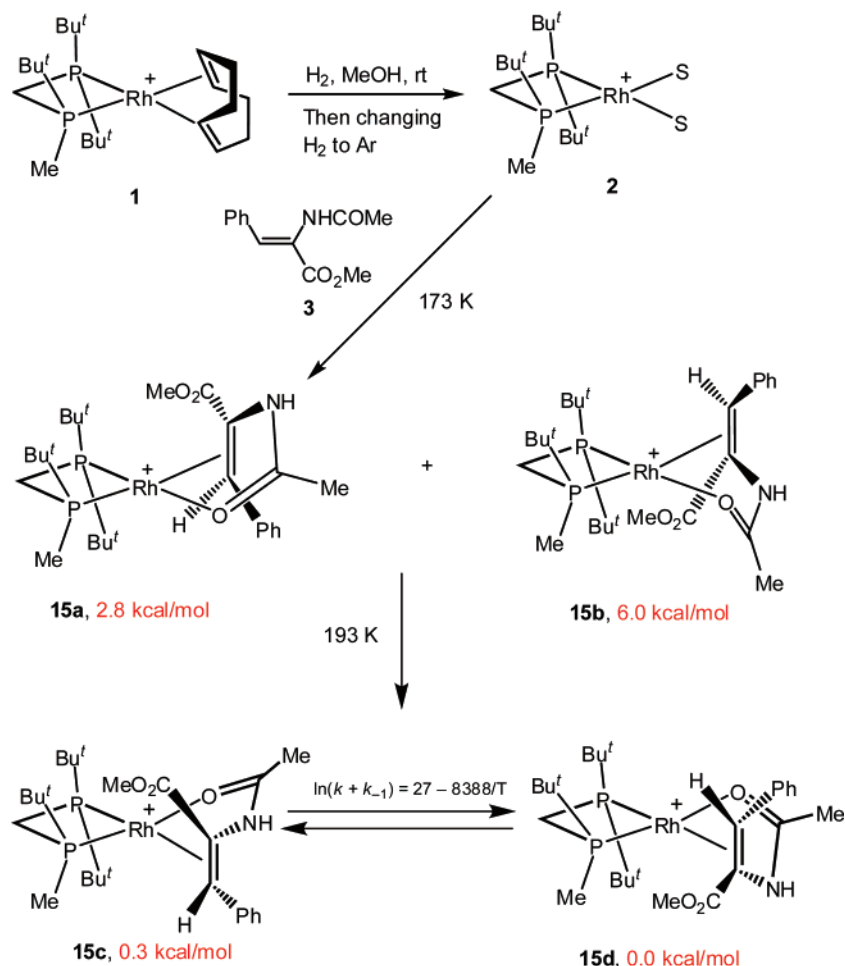
15b,c (vide infra) occurred rapidly at temperatures above −100 °C, and hence, we were unable to analyze their spectra separately. In the ¹³C NMR spectrum acquired at −100 °C, we detected a broad signal at $\delta = 78.0$ belonging to the β-carbon of the double bond in **15a,b** (controlled by the experiment with β-labeled **3**), which indicates that the double bond is coordinated to rhodium in **15a,b**. Moreover, whereas the signal of the carbonyl carbon from the carboxyl group was only slightly shifted from the corresponding signal of **3** ($\Delta\delta = 2.1$), the amido carbonyl signal demonstrated a significant downfield shift ($\Delta\delta = 13.9$). These data, are sufficient to conclude that kinetic products **15a,b** have structures of chelate catalyst−substrate complexes. Further experimental and computational results (vide supra) enabled us to conclude that the double bond in **15a,b** is coordinated to the rhodium from the side of the non-"chiral" phosphorus atom.

Initially formed kinetic products **15a,b** rearranged slowly at −100 °C, yielding two further products **15c** and **15d**. Initially, **15d** slightly predominated in the reaction mixture: the ratio **15c**:**15d** was in the range of 1:1 to 1:1.4 in different experiments. In each experiment, the ratio did not change significantly if the sample temperature was kept below −40 °C (Figure 1); above this temperature, the equilibrium ratio **15c**:**15d** was established. The equilibrium concentrations changed slightly from 1:0.85 at 25 °C to 1:0.70 at −40 °C; linearization of the ln K versus inverse temperature in the temperature range of −40 °C to 25

°C gave the following parameters of equilibrium between **15c** and **15d**: $\Delta H = 0.72$ kcal mol⁻¹ and $\Delta S = 2.0$ cal mol K⁻¹.

At temperatures above 20 °C, dynamic effects caused by the interconversion of **15c** and **15d** were clearly seen in the NMR spectra of the equilibrium mixture (Figure 2). From Figure 2, it is also clear that the intramolecular exchange between **15c** and **15d** is significantly faster than the exchange pathway involving complete dissociation. This implies that partially dissociated species with coordinated carbonyl and dissociated double bond are involved in the equilibrium. The activation parameters of the interconversion (Scheme 2) were determined from a series of phase-sensitive ¹H−¹H EXSY spectra.

The ¹H NMR spectrum of the equilibrium mixture of **15c** and **15d** in deuteriomethanol was completely resolved at 300 MHz, enabling assignment of the signals via routine 2D correlation techniques. The chemical shifts of the double bond carbons and of the amido carbonyl carbon confirmed that both compounds are chelating catalyst−substrate complexes. From ³¹P−¹H correlation spectrum, the signals of *t*-Bu groups and methyl were assigned to each particular isomer. Moreover, the *t*-Bu groups for each isomer could be clearly distinguished as those belonging to the phosphorus atoms with either two *t*-Bu groups or with *t*-Bu and Me group ("chiral" phosphorus).

Furthermore, in the phase-sensitive NOESY spectrum of the equilibrium mixture, positive NOEs were observed between =C−H proton and Me as well the *t*-Bu group from the same
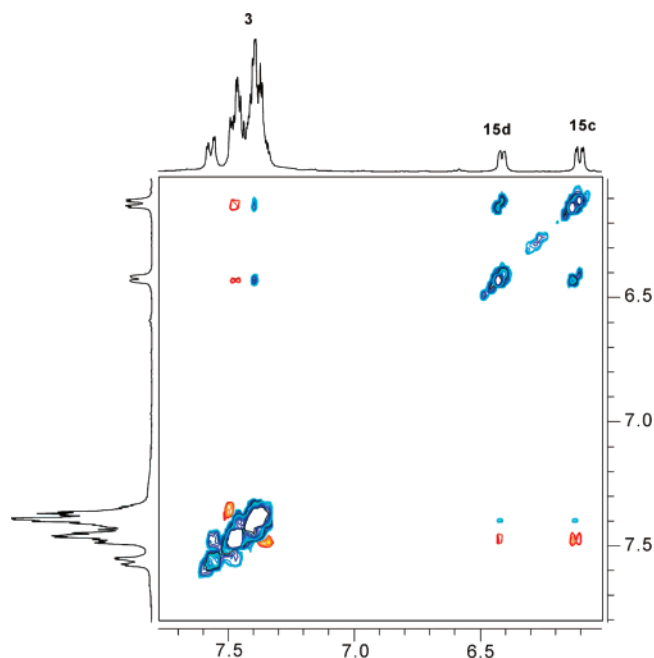
Figure 2. Section plot of phase sensitive 2D ^{1}H–^{1}H EXSY spectrum (300 MHz, CD$_3$OD, 293K) of the equilibrium mixture containing **15c**, **15d** (in fast equilibrium with **16d**, vide infra) and free substrate **3** (concentration of **3** was approximately equal to those of **15c** and **15d**). The exchange cross-peaks between the olefinic protons of **15c** and **15d** and between the *ortho*-aromatic protons of **15c** and **15d** are much more intensive than the exchange cross-peaks of the olefinic protons of **15c** and **15d** with the olefinic proton of **3**. Hence, mainly the exchange between **15c** and **15d** occurs intramolecularly.

phosphorus atom of **15a** and only between =C–H proton and the *t*-Bu group belonging to the chiral phosphorus atom of **15b**. These data are sufficient for assigning the structures of **15a,b**, as shown in the Figure 3; the NOEs observed for the CO$_2$Me groups give additional support for the assignment.
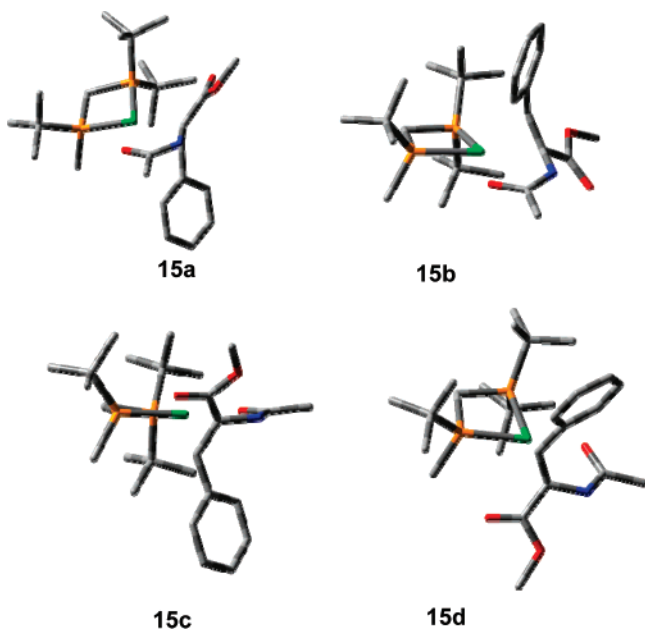
2.2.2. Computational Study of Complexes 15a–d. We have optimized the geometries of four possible diastereomers **15a–d** on the B3LYP/SDD level of theory (Figure 4). The results are in good accordance with the experimental data. The two most stable isomers are **15c** and **15d** with almost equal stabilities; **15a** and **15b** are 6.0 and 2.8 kcal/mol less stable, respectively
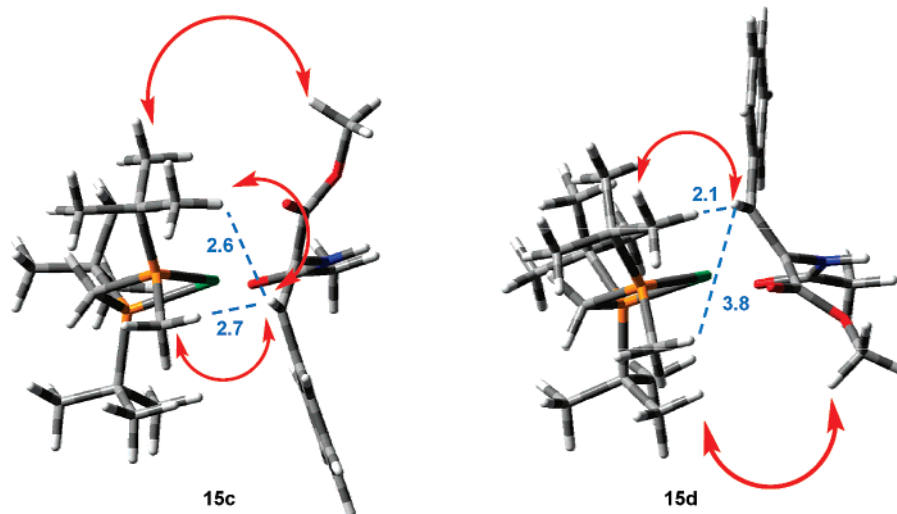
(Scheme 1). The coordination mode of the double bond is very similar in all the four isomers: α-carbon atom lies almost perfectly in the P–Rh–P plane, whereas β-carbon atom is invariably out of the plane. Furthermore, in all optimized structures, the double bond is not perpendicular to the P–Rh–P plane but is bent with its CHPh end toward the chelate cycle (the deviation from perpendicular orientation is close to 20° in all the four isomers). This bending of the double bond well explains the significant difference in energies between **15a** and **15b**. Indeed, the bending of the double bond results in close contact between the phenyl ring and the *t*-Bu group in **15b**, but is avoided in **15a** since the phenyl group is located near the relatively small methyl group. Nevertheless, **15a** is still almost 3 kcal/mol less stable than either **15c** or **15d**, demonstrating the general disadvantages of the double bond coordination near the non-"chiral" phosphorus atom having two *t*-Bu substituents. This is a result of inevitable close contacts of the *t*-Bu groups even with the non-substituted side of the double bond (the distance between =CH proton and *t*-Bu group is less than 2 Å in **15a**).

2.2.3. Low-Temperature Equilibrium of Catalyst–Substrate Complex 15d. In the temperature range between 173 and 243 K, the NMR spectra of **15d** exhibit characteristic line shape dependence, indicating rapid equilibrium of two species (the ratio is approximately 4:1 at 173 K). On the other hand, the spectra of **15c** remain unchanged in the same temperature range (Figure 5). The equilibrium is quite fast; qualitative estimation of line shape changes suggests that the activation barrier is approximately 6 kcal/mol. We conclude that this species is partially dissociated complex **16d** (Scheme 3); the existence of rapid equilibrium for such a species at ambient temperature is evident from the fast intramolecular exchange between **15c** and **15d** (vide supra). Since **15c** can interconvert with **15d** at temperatures above −40 °C (equilibrium concentrations of **15c** and **15d** are achieved after approximately 1 h at −30 °C), **15c** must also be capable of undergoing ligand exchange reaction with methanol to yield partially dissociated species **16d** (or its easily available rotamer, e.g., **16c**, see Scheme 3), so that the interconversion between **15c** and **15d** could proceed while keeping the carbonyl group coordinated. How-


Figure 3. Most important NOE's (red arches) for the structural assignment of **15c** and **15d**. The geometries were optimized on the B3LYP/SDD level of theory. The numbers show the distance in angstrom to the nearest protons in Me and *t*-Bu groups in the optimized structures.

15a   **15b**

15c   **15d**

Figure 4. Optimized geometries of the catalyst–substrate complexes **15a-d** (B3LYP/SDD). Hydrogens are removed for clarity.
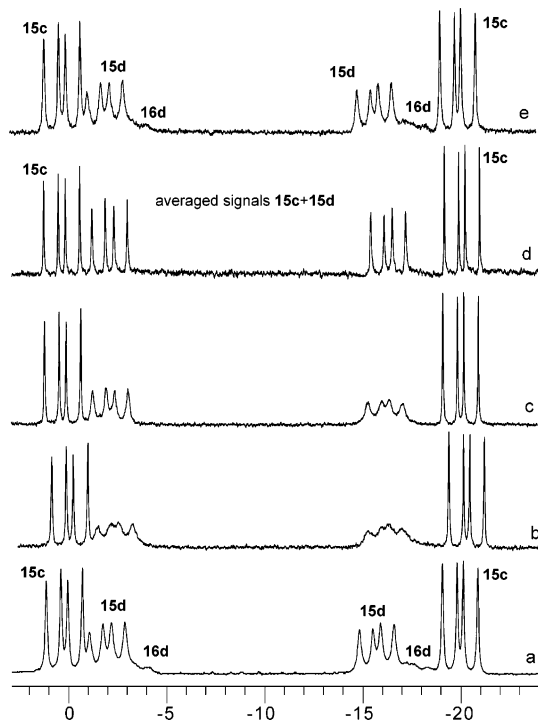

Figure 5. Temperature dependent ^{31}P NMR spectrum of the sample containing nonequilibrium concentrations of **15c** and **15d** (ratio **15c** : **15d** was approximately 1 : 1 in this sample): a) at −100 °C; b) at −90 °C; c) at −80 °C; d) at −60 °C; e) at −100 °C (recooled).

ever, the activation barrier of this ligand exchange reaction in the case of **15c** is apparently much higher than that of **15d**.

2.2.4. Computational Study of Insertion of Methanol Molecule into 15c,d. We attempted to support the above conclusion computationally. Apparently, when the double bond dissociates, the resulting free coordination space is immediately occupied by a methanol molecule. Hence, computations were based on the structures of **15c,d** having one methanol molecule bonded via the hydrogen bond. We also realized that in the real system, the situation is much more complicated due to the

Scheme 3. Intramolecular Interconversion of **15c**·MeOH and **15d**·MeOH
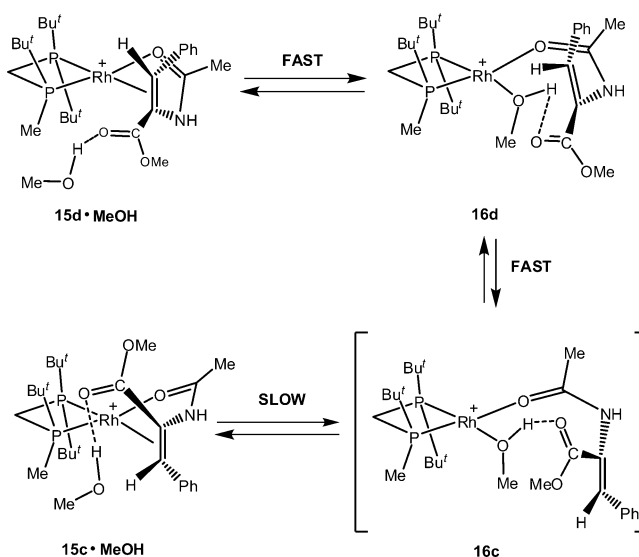

presence of numerous readily available methanol molecules. Thus, our computations showed that attaching the first, second, and third methanol molecule to **15d** is exothermic at approximately 10 kcal mol^{-1} each. Hence, one could not hope to obtain realistic values of the activation barriers for any steps with solvent participation without having to involve numerous methanol molecules in computations. However, increasing the number of computed methanol molecules attached to the Rh complex leads to a dramatic increase in the number of possible isomers that differ in position and binding mode of the methanol molecules. This and other complications prevented previous workers from considering solvent participation in theoretical studies of asymmetric hydrogenation.[16–20] Nevertheless, these effects must be the same for different isomers of the Rh complexes. Hence, by comparing the relative stabilities of the computed transition states, one can elucidate the reasons for the relative reactivities of the corresponding intermediates.

We have located the structures of **15d**·MeOH and **16d** connected through transition state **TS1**, (Figure 6). The two intermediates with chelate coordination of the substrate **15d**·MeOH and with only carbonyl group coordinated **16d** have very similar energies that is in accord with the experimental observation of the equilibrium between **15d** and **16d**. The computed value of the activation energy (11.1 kcal mol^{-1}) is approximately twice as high as the experimentally observed barrier. This deviation is probably a result of using only one methanol molecule in computations.

Insertion of the methanol molecule occurs from the side of the nonhindered quadrant. This transformation is facilitated by the hydrogen bonding to the polar methoxycarbonyl group that is maintained throughout the whole process (see structure of **TS1** in Figure 7). Use of the same reaction pathway for the insertion of a methanol molecule into **15c**·MeOH is impossible due to the large hindrance from the *t*-Bu group. In order to realize the insertion, the methanol molecule must approach sideways to minimize interference with the hindered quadrant and to maintain contact with the methoxycarbonyl group (see structure of **TS2** in Figure 7). As a result, the activation barrier of the methanol insertion into **15c**·MeOH is more than 2-fold higher than that into **15d**·MeOH (Figure 6).
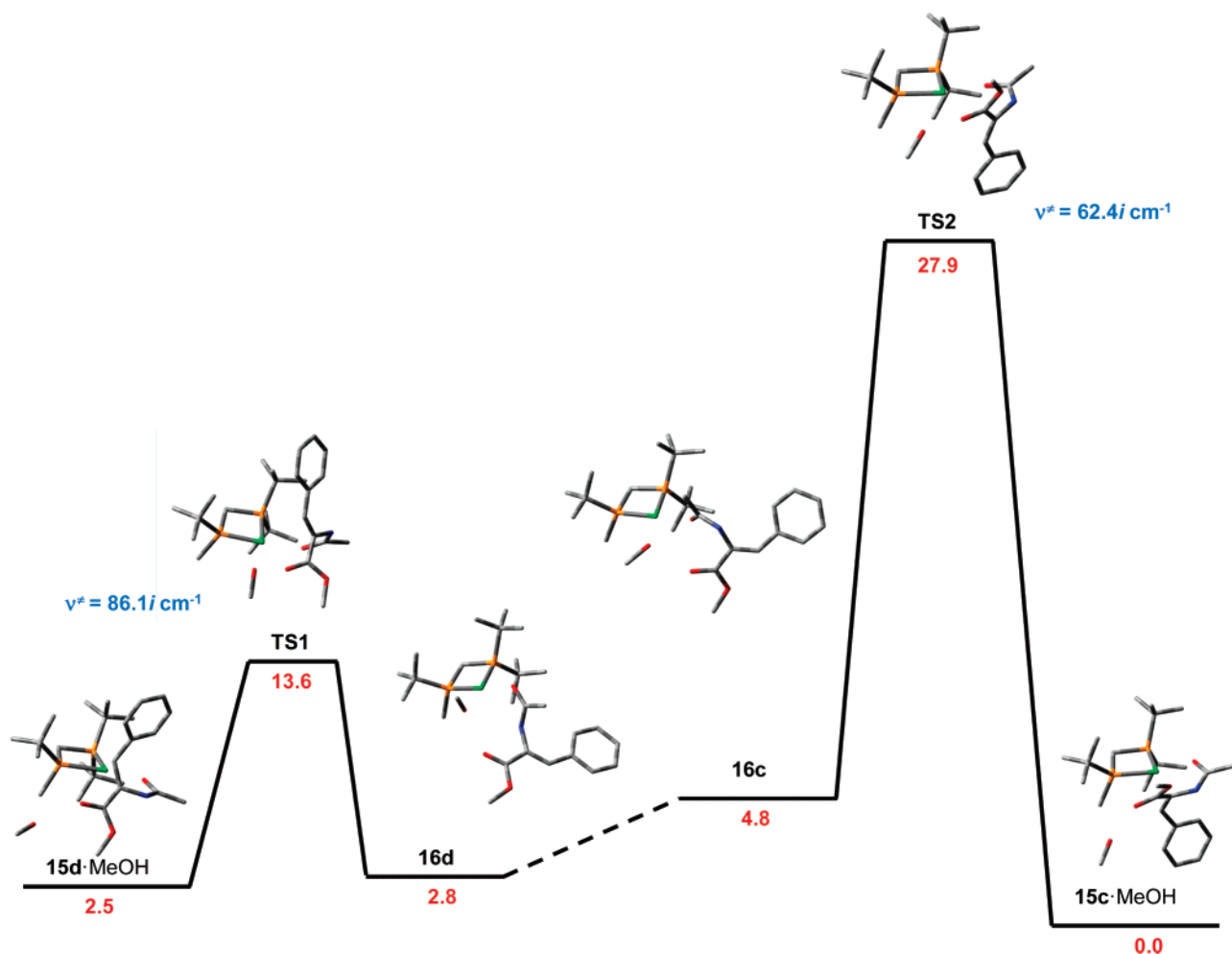
Figure 6. Schematic energy profile for the interconversion of solvated catalyst−substrate complexes **15c,d** through partially dissociated species **16c,d** computed on the B3LYP/SDD level of theory.
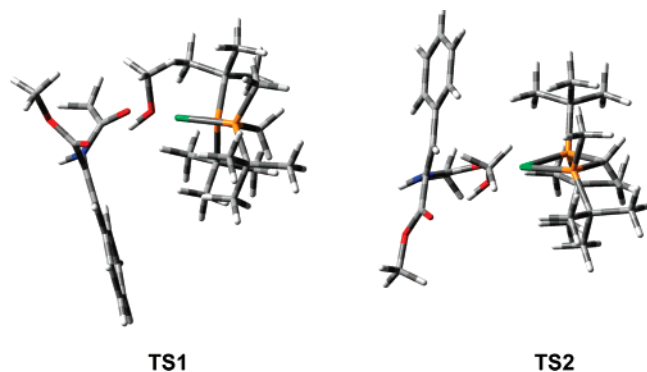
Figure 7. Structures of **TS1** and **TS2** optimized on the B3LYP/SDD level of theory.

Apparently, **15a,b** can undergo methanol insertion via transition states resembling **TS2**. The low activation barriers for these reactions (line shape changes in the ^{31}P NMR spectrum suggest that these equilibria are still faster than the case of **15d**) can be explained by the relative instability of these complexes. Furthermore, the experimental data indicate the activation barriers of the rearrangements of **15a,b** to **15c,d** to be low, since the rearrangements proceed at a reasonable rate even at −100 °C. However, **15a,b** evidently are not equilibrating with **2** in the temperature range of −100 to −80 °C (see Figure 1). Hence, the relatively rapid equilibrium of partially dissociated species

Scheme 4. Equilibration of Partially Dissociated Catalyst−substrate Complexes
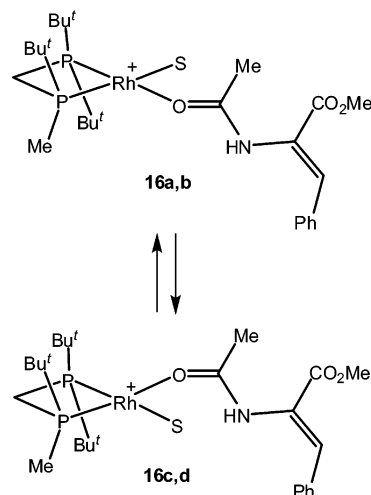
16a,b and **16c,d** must be possible. That, in turn, requires reorientation of the carbonyl group without complete dissociation of the substrate (Scheme 4).

Interesting information presents also selective formation of the kinetic products **15a,b** in the low-temperature experiments. This fact demonstrates that the coordination of **3** is stepwise and begins from the coordination of the carbonyl group which

Scheme 5. Selective Hydrogenation of Different Catalyst−substrate Complexes
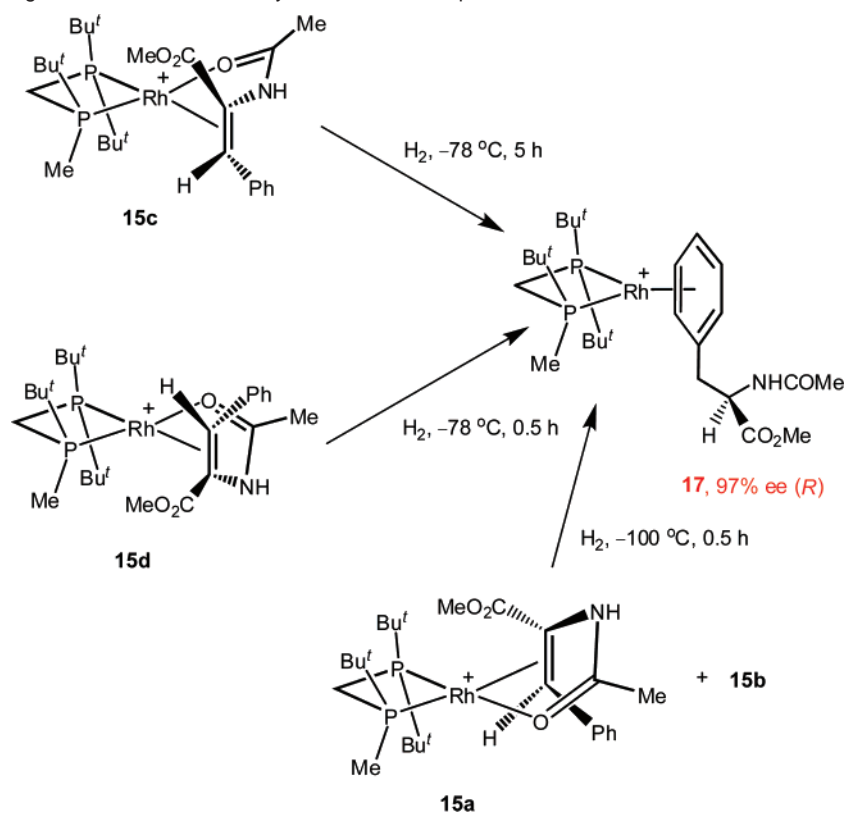
chooses initially the least hindered side of the molecule. Hence, in the catalytic conditions when the catalyst **2** is released from the catalytic cycle to bind the next molecule of the substrate, the first intermediates are **16a,b**; and if the hydrogenation of these semi-dissociated species is fast enough it might (at least partially) occur without prior chelating coordination.

2.2.5. Low-Temperature Hydrogenation of Catalyst− Substrate Complexes. Having established the details of the equilibrium between various catalyst−substrate complexes formed from **2** and **3**, we investigated several regimes of low-temperature hydrogenation to gain an insight into the relative reactivity of isomeric catalyst−substrate complexes toward hydrogen. Three experiments were designed (Scheme 5).

In the first experiment, we added an equivalent amount of **3** to a solution of **2** at −100 °C and immediately hydrogenated the reaction mixture for 30 min while keeping the temperature at −100 °C. According to Figure 1, under these conditions, the reaction mixture contained only **15a,b** together with nonreacted **2** and **3**. After hydrogenation, hydrogen gas was replaced with argon to eliminate the possibility of any hydrogenation at higher temperatures. Then, the sample was quenched and the reaction product was analyzed. NMR analysis showed that 40% of **3** was hydrogenated; the ee of the product was 97% (*R*).

In the second experiment, an equilibrium mixture of **15c** and **15d** (equilibrated with **16d**) was prepared at 25 °C. Then, it was cooled to −78 °C and hydrogenated at this temperature with regular control by monitoring the ^{31}P NMR spectrum (Figure 8). After hydrogenation for 30 min, the equilibrium mixture of **15d** and **16d** was selectively hydrogenated, whereas **15c** remained unreacted (Figure 8c). Quenching the mixture at this stage yielded a reaction product (conversion was again 40%) with 97% ee (*R*).

In the third experiment, the hydrogenation was continued from the point where it was stopped in the previous experiment. Preparing the sample with the ^{31}P NMR spectrum as in Figure 8c, we continued hydrogenation at −78 °C while monitoring the progress of the reaction with ^{31}P NMR. As can be seen from Figure 8, **15c** was completely hydrogenated after 5 h at this temperature. The reaction product (conversion 100%) recovered from this experiment had again 97% ee (*R*).

That the same optical purity of the hydrogenation product was obtained in all three experiments is quite remarkable. Especially meaningful is the last experiment: since **15c** has an *Re*-coordinated double bond, it would be expected to produce an *S*-product if it were hydrogenated directly. However, this is clearly not the case. Moreover, the rate of equilibrium between **15c** and **15d** (vide supra) implies that at −78 °C, the temperature at which both were hydrogenated, no appreciable interconversion occurs. To check this point more carefully, we again prepared a sample with **15d** being selectively hydrogenated (as in Figure 8c, see Figure 9) and kept it for 6 h at −70 °C. As can be seen from Figure 9, no traces of **15d** could be found in the ^{31}P NMR spectrum. On the other hand, as can be expected from the already known rate of interconversion, the formation of **15d** from **15c** occurred quite rapidly at −30 °C.

Thus, we conclude that the formation of *R*-hydrogenation product when **15c** was hydrogenated cannot be explained by its prior isomerization to **15d**, since this isomerization does not occur under the conditions of the experiment. Nevertheless, the hydrogenation of **15c** must be preceded by a process eliminating the stereodiscriminating coordination of the prochiral double bond in **15c** to allow formation of the *R*-product. Apparently, the hydrogenation of **15c** occurs through the intermediacy of nonchelating catalyst−substrate complex **16c** (Scheme 6). It is
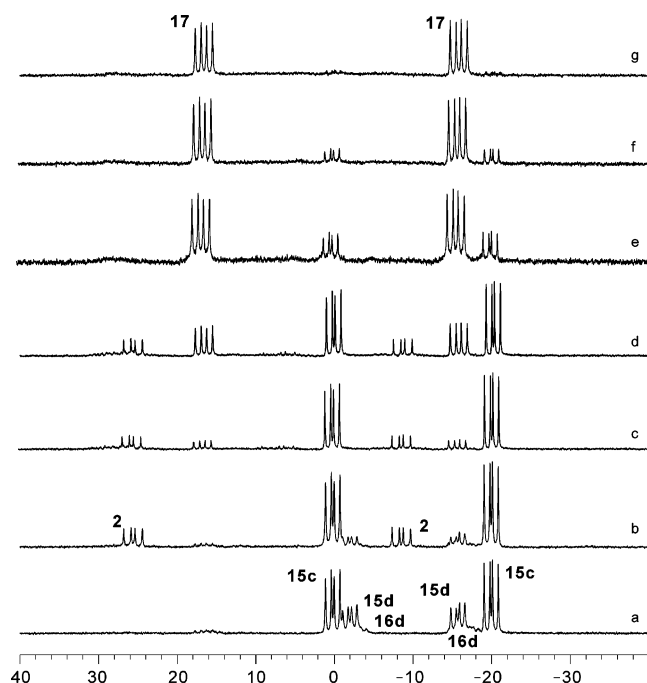
Figure 8. Evolution of the ^{31}P NMR (62 MHz, CD$_3$OD, −90 °C) of the sample originally containing the equilibrium mixture of **15c** and **15d**: a) H$_2$ admitted to the sample instead of Ar at −78 °C, then the sample was cooled to −100 °C and placed into the probe precooled to −100 °C, the spectrum taken at −90 °C; b) after 10 min hydrogenation at −78 °C (handling of the sample is same further on); c) after additional 20 min hydrogenation at −78 °C; **15d** is completely removed; d) after additional 1 h hydrogenation at −78 °C; e) after additional 1.5 h hydrogenation at −78 °C; f) after additional 1 h hydrogenation at −78 °C; g) after additional 1 h hydrogenation at −78 °C, the total hydrogenation time was 5 h, the product obtained from this sample was of 97% ee) (*R*).

quite reasonable to suggest that **16c** would be more reactive toward dihydrogen than much more crowded **15c**. It has been shown that the steric hindrance plays an important role in the hydrogenation step of the catalytic cycle in Rh-catalyzed asymmetric hydrogenation.[16]

Moreover, quite remarkable is the straightforward correlation between the ease of dissociation of the double bond and the reactivity of the corresponding catalyst−substrate complex. Thus, **15d** is in rapid equilibrium with approximately 20% of **16d**, and the corresponding equilibria of **15a,b** are even faster, indicating that the partially dissociated species generated from these catalyst−substrate complexes are readily available, even at −100 °C, and their hydrogenation can be rapidly accomplished at this temperature. Unfortunately, the equilibrium is so fast that it was beyond our experimental techniques to check if **16d** can be selectively hydrogenated before its equilibrium with **15d** is re-established at −100 °C. Nevertheless, the relative ease of hydrogenation of **15a−d** is evidently correlated with their partial dissociation rates, and the exactly equal optical yields obtained in the three hydrogenation experiments suggest that, in all three cases, hydrogenation proceeded through the same semi-dissociated species **16** (the difference between **16a** and **16b** (as well as between **16c** and **16d**) is purely conformational, and these pairs can equilibrate either, see Scheme 4). At a later stage of the catalytic cycle, the double bond of the substrate must have become re-coordinated to ensure the occurrence of enantioselective catalytic hydrogenation. Unfortunately, no further intermediates were detected in low-
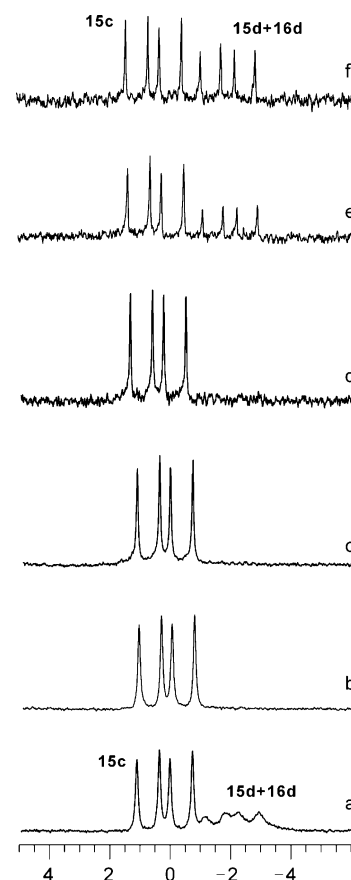
Figure 9. Section plots of the ^{31}P NMR spectra of the sample initially containing the equilibrium mixture of **15c** and **15d**: a) starting spectrum at −90 °C; b) after 30 min hydrogenation at −78 °C, spectrum taken at −90 °C; c) sample was kept for 5 h at −70 °C and the spectrum was taken at this temperature; d) immediately after raising the temperature to −30 °C; e) after 6 min at −30 °C; f) after 30 min at −30 °C.

Scheme 6. Hydrogenation of **15c**
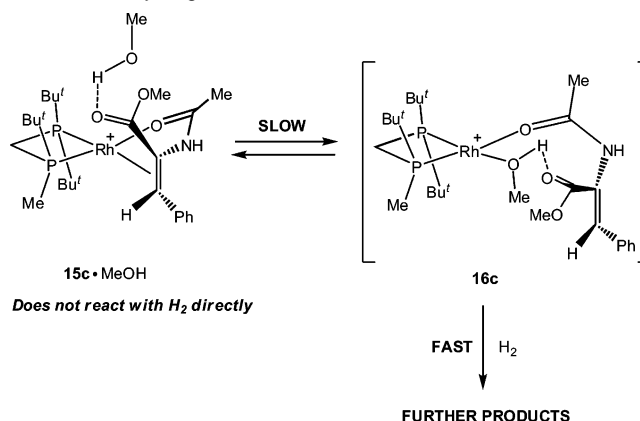
temperature hydrogenation experiments, and hence, we addressed this problem computationally.

It should be noted that the equilibration of the catalyst−substrate complexes with the *semi*-dissociated species is not unique feature of the system under study. Thus, Brown et al. have shown the existence of similar species through intramolecular excitation transfer in ^{31}P NMR of the diastereomeric DIPAMP−Rh complexes of α-dehydroamino acids.[33,34] Impor-
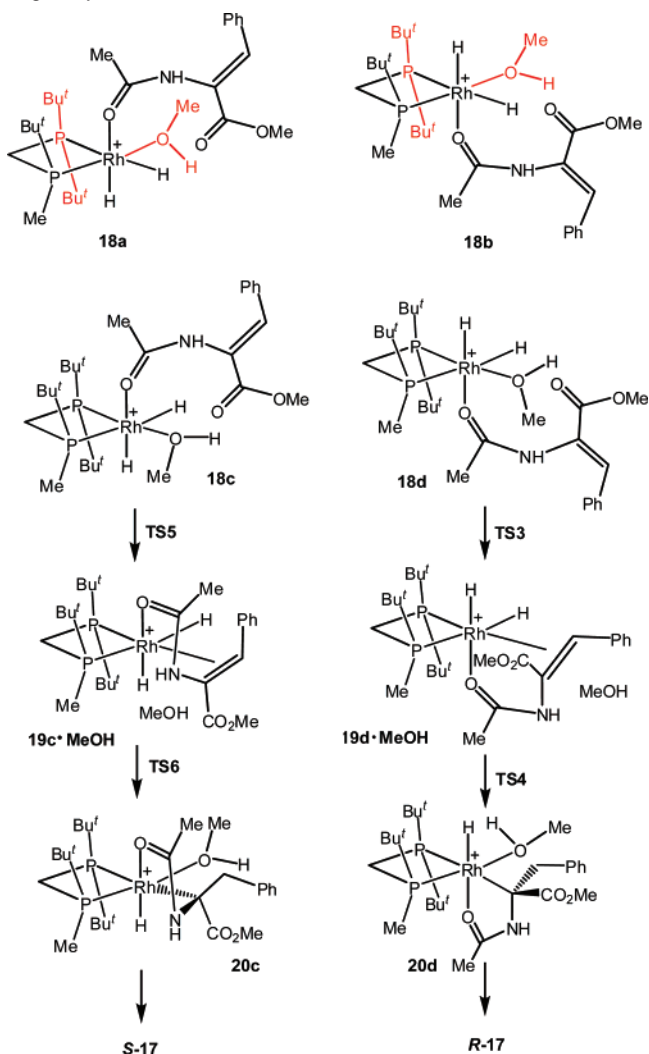
(33) Brown, J. M.; Chaloner, P. A.; Morris, G. A. *J. Chem. Soc., Chem. Commun.* **1983**, 664.

tantly, it has been also recognized that the semi-dissociated species have the potential to capture dihydrogen, thus affecting the particular details of the catalytic cycle.[33] The same conclusions were later made from the 2D $^{31}P-^{31}P$ EXSY studies of the DIPAMP,[35] CHIRAPHOS,[35] and 1-((2-methoxyphenyl)-phenylphosphino)-2-diphenylphosphinoethane[36] Rh complexes of **3**, as well as of Rh-BisP* complexes of enamides.[27c] Similarly, the dramatic line shape changes in the ^{31}P NMR of the seven-membered ring chelates of Rh-bis(phosphinites) are also explained by fast intramolecular interconversion of the corresponding catalyst–substrate complexes that involves the intermediacy of the semi-dissociated species.[37] Thus, the pathway involving the hydrogenation of the species with a non-coordinated double bond might be operative in other catalytic systems helping to avoid the high activation barriers of oxidative addition in square planar catalyst–substrate complexes. It is important therefore to understand how and when the stereoselection can occur if the stereodiscriminating coordination of the double bond is lost during the oxidative addition step.

2.2.6. Computational Study of Association and Migratory Insertion Steps. From previous computational studies of Rh-catalyzed asymmetric hydrogenation, it is known that the oxidative addition of dihydrogen to an Rh complex is preceded by the formation of molecular hydrogen complexes.[16–20] Moreover, in some reaction pathways, this step has a very high activation barrier due to the steric hindrance provided by the coordinated substrate. However, these complications are avoided in our system as the hydrogenation proceeds through partially dissociated species **16** that is much less hindered, and different modes of H_2 addition become equally possible. Besides, intermediates with non-coordinated double bonds can easily interconvert, as is seen in the experimentally observable transformation of **16a,b** into **16b,c** that occurs rapidly at −100 °C (Scheme 4). Hence, we have skipped in our analysis the stages preceding double bond recoordination followed by migratory insertion, since they cannot possibly contribute to the generation of enantioselectivity.

There are numerous possible isomers of partially coordinated dihydride intermediates that theoretically can lead to multiple reaction pathways. However, using the results of previous theoretical studies and our own conclusions, we can reduce the problem of the enantioselectivity to the difference between only two pathways. Since we start the analysis from easily interconvertible intermediates with non-coordinated double bonds, any configuration of the chelate dihydride can be achieved through the double bond coordination preceding the migratory insertion step that allows the system to choose the lowest available barriers. Furthermore, although previous studies of other catalytic systems considered the possibility of migratory insertion occurring through dihydride intermediates with apically coordinated double bonds, we found it absolutely impossible to accommodate the molecule of **3** in such a way with our catalyst. The large spherical *t*-Bu groups inevitably collide with either the phenyl or the methoxycarbonyl group, and approaches

(34) Brown, J. M.; Chaloner, P. A.; Morris, G. A. *J. Chem. Soc., Perkin Trans. II* **1987**, 1583.
(35) Bircher, H.; Bender, B. R.; von Philipsborn, W. *Magn. Reson. Chem.* **1993**, *31*, 293.
(36) Ramsden, J. A.; Claridge, T. D. W.; Brown, J. M. *J. Chem. Soc., Chem. Commun.* **1995**, 2469.
(37) Kadyrov, R.; Freier, T.; Heller, D.; Michalik, M.; Selke, R. *J. Chem. Soc., Chem. Commun.* **1995**, 1745.

Scheme 7. Two Alternative Pathways for the Association and Migratory Insertion

to such configurations from the *semi*-coordinated complexes are evidently unrealistic.

This leaves four isomers **18a–d** for consideration (Scheme 7). However, we did not think about the possibility of the reaction taking place through **18a,b** as that would imply coordination of the double bond near the non-"chiral" phosphorus atom that is evidently disfavored (e.g., see above the relative stabilities of corresponding catalyst–substrate complexes). Hence, the problem of the origin of enantioselectivity can be reduced in the present case to the analysis of the double bond recoordination and the subsequent migratory insertion starting from two *semi*-coordinated dihydrides **18c,d**, which are precursors of *S*- and *R*-products, respectively (Scheme 7).
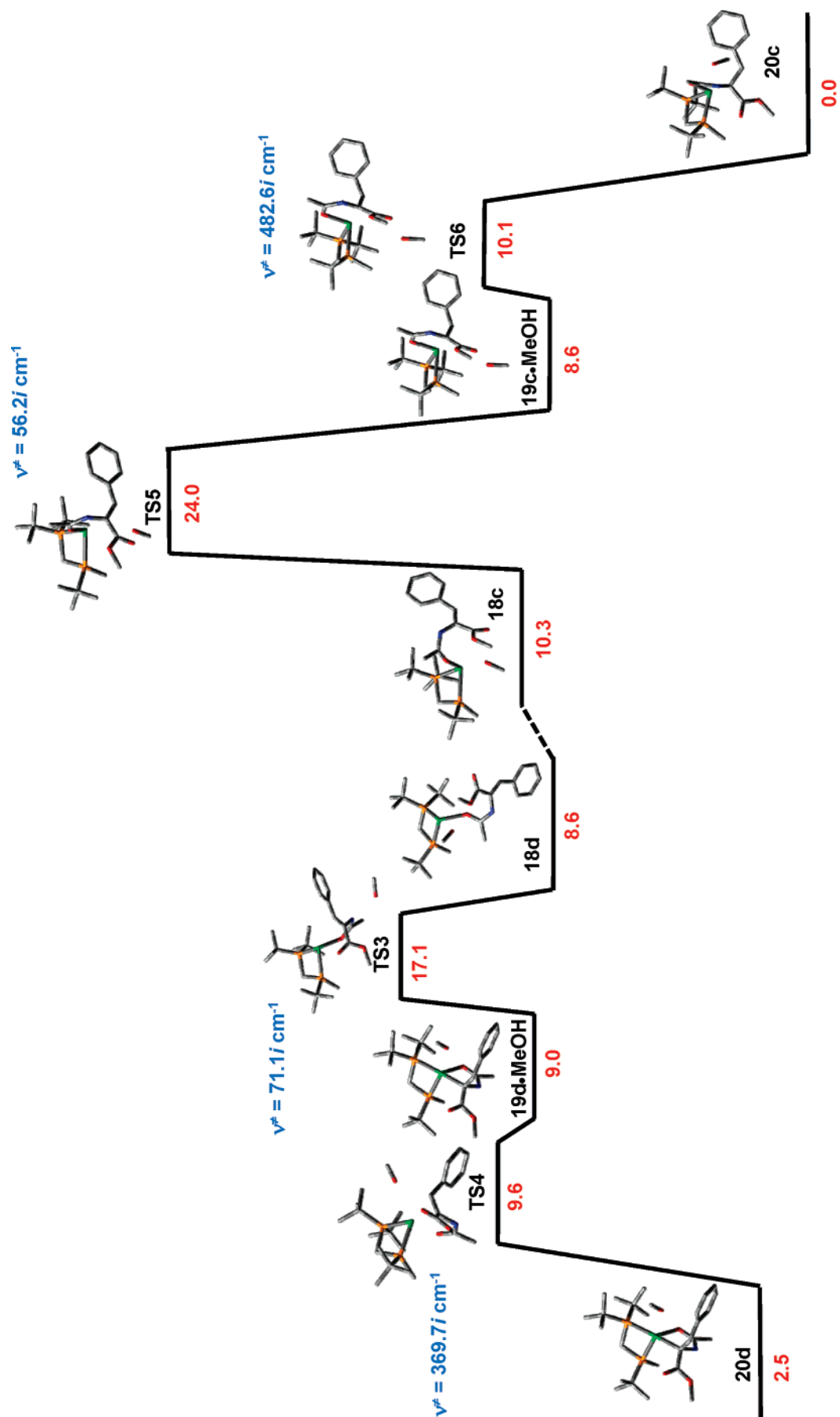
Similarly to the computations performed for the catalyst–substrate complexes, we used for calculations of association and migratory insertion steps real compounds with one methanol molecule either coordinated to the free coordination space at rhodium or hydrogen-bonded to the carboxyl group of the substrate. According to previous research, the *R*-configuration of the hydrogenation product together with the catalyst configuration implies that the first hydrogen is transferred to the β-carbon atom of the double bond, leading to the formation of α-monohydride intermediate. Hence, we looked for reaction pathways converting nonchelated dihydride intermediates **18c,d**

Figure 10. Alternative pathways for the association and migratory insertion steps computed on the B3LYP/SDD level of theory.
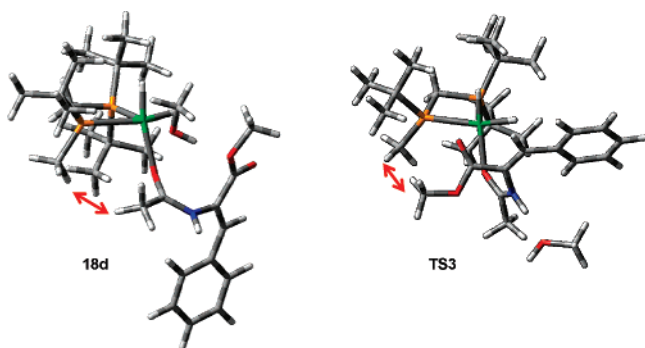
Figure 11. Structures of the nonchelating dihydride **18d** (left) and the transition state **TS3** (right) optimized on the B3LYP/SDD level of theory. The arrows indicate relatively close contacts between the methyl groups that would make impossible the same association pathway in the case of **18c** (with the P–Bu^t group instead of the P–Me).

into chelated species **19c,d**, which are direct precursors of corresponding α-monohydride intermediates **20c,d** (Scheme 7).

We found several transition states for the association step that converts various conformations of open dihydride **18d** into chelate dihydride intermediate **19d**. One of them, viz. **TS3** (Figure 10), had significantly lower energy (7–12 kcal/mol) than the others. The transformation of **18d** into **19d·MeOH** implies changing the lobe of the oxygen atom used to form the coordination bond with rhodium with simultaneous pushing of the methanol molecule out of the coordination sphere of rhodium through transition state **TS3**.

This process requires much activity in the single nonhindered quadrant and cannot be therefore paralleled in the association of the double bond leading to **19c·MeOH** (Figure 11). In this case, the lowest activation barrier was found for the process in which the methanol molecule is pushed out through the nonhindered quadrant via **TS5** that is 6.9 kcal/mol higher in energy than **TS3**. Apparently, this difference is the origin of the enantioselectivity, since the activation barriers for the migratory insertion step in both pathways are very low and transition states **TS4** and **TS6** are almost equally stable.

It is appropriate to note that, recently, we directly observed the operation of that kind of enantioselection on another three-hindered-quadrant catalyst, dirhodium complex of tetraphosphine ligand.[15] In that case, it was possible to observe the initial formation of nonchelating tetrahydride **22** when tetrahydride **21** was reacted with **3** at −100 °C. Although **22** had the catalyst, activated hydrogen, and the substrate combined in one molecule, it did not undergo migratory insertion unless it rearranged to isomer **23** that immediately gave the corresponding "monohydride" **24** (Scheme 8). That is the direct analogy to the transformation **18c → 18d → 19d·MeOH**. It illustrates that, although the intermediate **22** with incorrect configuration of Rh is generated quantitatively, it does not undergo migratory insertion due to its inability to coordinate the double bond effectively. Migratory insertion occurs only when the isomerization to **23** becomes possible, providing the configuration appropriate for the effective double bond coordination.

3. Conclusions

The Rh complex of (*R*)-(*tert*-butylmethylphosphino)(di-*tert*-butylphosphino)methane (**1**) was the first reported catalyst for the Rh-catalyzed asymmetric hydrogenation that must be considered as having three hindered quadrants. The present

Scheme 8. Direct Experimental Observation of the Formation of Nonchelating "dihydride" Complexes in the Reaction of the Dirhodium Tetraphosphine Solvate Dihydride with **3**[15]
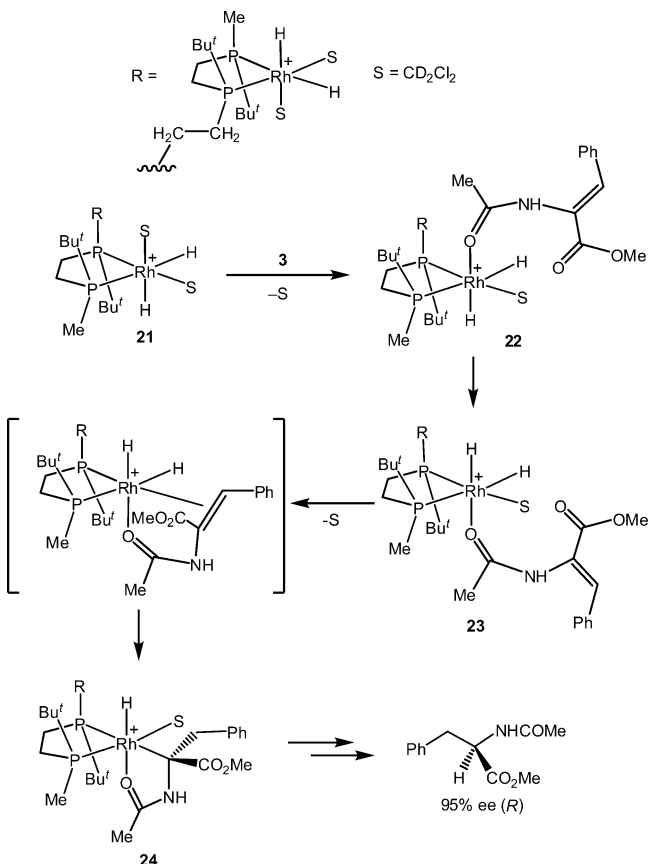
mechanistic study demonstrated and emphasized the productivity of this kind of ligand design. The non-chiral half of the catalyst does not contribute to the flux of catalysis because the approach of the prochiral double bond from that side is effectively blocked. We have confirmed that this conclusion is valid for representative substrates **3**–**14** and will report details of these studies elsewhere.

Further, we showed that in the catalytic system containing **2** as a catalyst and **3** as a substrate, the reactivity of the catalyst–substrate complex toward dihydrogen is correlated with the ease of its partial dissociation. Moreover, the absolutely equal ee's obtained from low-temperature hydrogenations of different catalyst–substrate complexes suggest that the enantioselection occurs at the later stage of the reaction. DFT calculations performed for a real catalytic system containing one methanol molecule give ample proof that the enantioselectivity is generated during the formation of an octahedral chelate complex, which precedes the irreversible migratory insertion step.

The relative ease of solvent insertion into the catalyst–substrate complexes is determined by the configuration of the Rh complex and of the double bond coordination mode: methanol easily displaces the double bond having a polar methoxycarbonyl group near the nonhindered quadrant. In turn, the relative availability of chelate dihydrides **19c·MeOH** and **19d·MeOH** from nonchelating species **18** is also evidently regulated by the configuration of the catalyst. Hence, the two phenomena, viz. relative reactivity of catalyst–substrate complexes and enantioselection, are correlated, but they do not stand in the cause-and-effect relationship. Any chiral information

acquired before the irreversible step[38] is lost due to the reversible dissociation of the double bond.

Studies of other related systems in line with the conclusions obtained in this work are underway in our laboratories.

4. Experimental Section

4.1. General Procedures. All reactions and manipulations were performed under dry argon atmosphere using standard Schlenk-type techniques. NMR experiments were carried out on a Jeol AL-300 spectrometer. Methanol-d_4 of grade "100%" (99.6% D) packed in sealed ampules was purchased from Cambridge Isotope Laboratories, Inc. Hydrogen (99.9999%, Tanuma Sanso) was used for mechanistic studies.

4.2. Solvate Complex 2. A solution of catalytic precursor **1** (20–40 mg) in 0.5 mL of CD$_3$OD was prepared in a 5 mm NMR tube under argon. Then, the sample was degassed by three cycles of freezing, pumping, and warming. The sample was cooled to −20 °C, 2 atm H$_2$ was admitted, and the temperature was raised to ambient. The sample was intensely shaken manually during the hydrogenation at ambient temperature. The progress of the hydrogenation was monitored by ^{31}P NMR; complete hydrogenation of the coordinated COD required 60–90 min at room temperature. After completion of the reaction, excess hydrogen was removed by several cycles of freezing, pumping, and warming. The thus-prepared solution of solvate complex **2** in deuteriomethanol was stable at ambient temperature.

4.3. Catalyst−Substrate Complexes 15. A solution of 1.5 equiv of methyl (Z)-α-acetamidocinnamate (**3**) in CD$_3$OD was added to the above prepared solution of **2** in CD$_3$OD either at ambient temperature or at −100 °C.

15c: ^{1}H NMR (300 MHz, CD$_3$OD, 20 °C): δ 1.14 (d, 9H, 3CH$_3$, $^3J_{HP}$ = 15 Hz), 1.23 (d, 9H, 3CH$_3$, $^3J_{HP}$ = 16 Hz), 1.47 (d, 9H, 3CH$_3$, $^3J_{HP}$ = 15 Hz), 1.39 (dd, 3H, CH$_3$, $^2J_{HP}$ = 9 Hz, $^4J_{HP}$ = 2 Hz,), 2.28 (s, 3H, CH$_3$), 3.2−3.3 (m, 2H, CH$_2$), 3.79 (s, 3H, CH$_3$O), 6.13 (dd, 1H, CH=, $^1J_{HRh}$, $^2J_{HP}$ = 7 and 2 Hz), 7.3−7.6 (m, 5H, C$_6$H$_5$); ^{13}C NMR (75 MHz, CD$_3$OD, 20 °C): δ 9.43 (d, CH$_3$, $^1J_{CP}$ = 25 Hz), 19.87 (dd, CH$_3$CON, $^4J_{CRh}$, $^5J_{CP}$ = 3 and 1 Hz), 27.38 (d, Bu^t, $^2J_{CP}$ = 4 Hz), 29.04 (d, Bu^t, $^2J_{CP}$ = 6 Hz), 29.4 (m, CH$_2$), 30.30 (d, Bu^t, $^2J_{CP}$ = 6 Hz), 34.49 (dd, C tert, $^1J_{CP}$ = 21 Hz, $^2J_{CRh}$ = 3 Hz,), 35.28 (dd, C tert, $^2J_{CRh}$ = 2 Hz, $^1J_{CP}$ = 14 Hz), 39.05 (dd, C tert, $^1J_{CP}$ = 9 Hz, $^2J_{CRh}$ = 2 Hz), 53.27 (OMe), 83.78 (d, CH=, $^3J_{CP}$ = 10 Hz), 90.25 (dd, $^3J_{CP}$ = 10 Hz, $^2J_{CRh}$ = 6 Hz), 130.10, 130.19, 130.73 (5CH, C$_6$H$_5$), 137.83 (C tert), 168.6 (d, C=O, $^4J_{CP}$ = 4 Hz), 188.4 (dd, NCO, $^3J_{CP}$ = 6 Hz, $^4J_{CRh}$ = 2 Hz); ^{31}P NMR (122 MHz, CD$_3$OD, 20 °C): δ −20.1 (dd, $^1J_{PRh}$ = 136 Hz, $^2J_{PP}$ = 89 Hz), 0.9 (dd, $^1J_{PRh}$ = 136 Hz, $^2J_{PP}$ = 89 Hz).

15d: ^{1}H NMR (300 MHz, CD$_3$OD, 20 °C): δ 1.18 (d, 9H, 3CH$_3$, $^3J_{HP}$ = 15 Hz), 1.29 (d, 9H, 3CH$_3$, $^3J_{HP}$ = 15 Hz), 1.46 (d, 9H, 3CH$_3$, $^3J_{HP}$ = 15 Hz), 1.62 (dd, 3H, CH$_3$, $^2J_{HP}$ = 9 Hz, $^4J_{HP}$ = 1 Hz,), 2.20 (s, 3H, CH$_3$), 3.2−3.3 (m, 2H, CH$_2$), 3.80 (s, 3H, CH$_3$O), 6.43 (dd, 1H, CH=, $^1J_{HRh}$, $^2J_{HP}$ = 5 and 2 Hz), 7.3−7.6 (m, 5H, C$_6$H$_5$); ^{13}C NMR (75 MHz, CD$_3$OD, 20 °C): δ 11.06 (d, CH$_3$, $^1J_{CP}$ = 25 Hz), 19.74 (dd, CH$_3$CON, $^4J_{CRh}$, $^5J_{CP}$ = 3 and 1 Hz), 26.99 (d, Bu^t, $^2J_{CP}$ = 5 Hz), 29.4 (m, CH$_2$), 29.70 (d, Bu^t, $^2J_{CP}$ = 5 Hz), 30.15 (d, Bu^t, $^2J_{CP}$ = 6 Hz), 33.68 (dd, C tert, $^2J_{CRh}$ = 3 Hz, $^1J_{CP}$ = 23 Hz), 36.31 (dd, C tert, $^1J_{CP}$ = 11 Hz, $^2J_{CRh}$ = 2 Hz), 37.56 (dd, C tert, $^1J_{CP}$ = 12 Hz, $^2J_{CRh}$ = 2 Hz,), 52.97 (OMe), 83.05 (d, CH=, $^3J_{CP}$ = 10 Hz), 89.68 (dd, $^3J_{CP}$ = 17 Hz, $^2J_{CRh}$ = 5 Hz), 129.75, 130.60 (5CH, C$_6$H$_5$), 130.84, 138.08 (C tert), 168.8 (d, C=O, $^4J_{CP}$ = 2 Hz), 189.2 (dd, NCO, $^3J_{CP}$ = 6 Hz, $^4J_{CRh}$ = 3 Hz); ^{31}P NMR (122 MHz, CD$_3$OD, 20 °C): δ −16.4 (dd, $^1J_{PRh}$ = 136 Hz, $^2J_{PP}$ = 81 Hz), −1.50 (dd, $^1J_{PRh}$ = 137 Hz, $^2J_{PP}$ = 81 Hz).

4.4. Hydrogenation Experiments. Due to the importance of temperature control for the conclusions of the present research, utmost care was given to maintain the temperature of the hydrogenation reaction. The temperature of the cooling bath was maintained at −78 °C (dry ice + acetone), and the sample connected to the rubber balloon with dihydrogen was manually kept inside the bath throughout the whole hydrogenation process. To enable the necessary mass transfer, the sample was intensely shaken manually. This technique was previously proven to be faultless; 100% conversion of a catalyst−substrate complex into a monohydride intermediate unstable below −85 °C was achieved via hydrogenation with the bath temperature set at −90 °C (see Gridnev, I, D.; et al. *J. Am. Chem. Soc.* **2001**, *123*, 5268). To account for the casual rise in temperature in the process of manual shaking, we carried out a control experiment that demonstrated the lack of interconversion between **4a** and **4b** at −70 °C.

5. Computational Details

Geometries of all stationary points were optimized using analytical energy gradients of self-consistent-field[39] and density functional theory (DFT).[40] The latter utilized Becke's three-parameter exchange-correlation functional[41] including the non-local gradient corrections described by Lee−Yang−Parr (LYP),[42] as implemented in the *Gaussian 03* program package.[43] All geometry optimizations were performed using the SDD basis set.[44] This approach is widely used for the recent computational studies of transition metal complexes and was shown to yield results conforming with experimental data in the works of our own[45] and of others.[46]

Supporting Information Available: NMR Charts, cartesian coordinates of the optimized structures, and complete ref 43. This material is available free of charge via the Internet at http://pubs.acs.org.

JA076542Z

(38) In the present case, it is probably reductive elimination, since monohydride **20d** is quite unstable and could not be detected.

(39) Pulay, P. In *Modern Theoretical Chemistry*; Schaefer, H. F., Ed.; Plenum: New York, 1977; Vol. 4, p 153.

(40) (a) Parr, R. G.; Yang, W. *Density Functional Theory of Atoms and Molecules*; Oxford University Press: New York, 1989. (b) Cheeseman, J. R.; Frisch, M. J.; Devlin, F. J.; Stephens, P. J. *Chem. Phys. Lett.* **1996**, *52*, 211.

(41) (a) Becke, A. D. *Phys. Rev. A* **1988**, *38*, 3098. (b) Becke, A. D. *J. Chem. Phys.* **1993**, *98*, 5648.

(42) (a) Lee, C.; Yang, W.; Parr, R. G. *Phys. Rev. B* **1988**, *37*, 785. (b) Miehlich, B.; Savin, A.; Stoll, H.; Preuss, H. *Chem. Phys. Lett.* **1989**, *157*, 200.

(43) Frisch, M. J.; et al. *Gaussian 03*, Revision B.05; Gaussian, Inc.: Pittsburgh PA, 2003.

(44) (a) Dunning, T. H., Jr.; Hay, P. J. In *Modern Theoretical Chemistry*; Schaefer, H. F., III, Ed.; Plenum,: New York, 1976; Vol. 3, p 1. (b) Leininger, T.; Nicklass, A.; Stoll, H.; Dolg, M.; Schwerdtfeger, P. *J. Chem. Phys.* **1996**, *105*, 1052.

(45) (a) Nakamura, I.; Bajracharya, G. B.; Wu, H.; Oishi, K.; Mizushima, Y.; Gridnev, I. D.; Yamamoto, Y. *J. Am. Chem. Soc.* **2004**, *126*, 15423. (b) Nakamura, I.; Mizushima, Y.; Gridnev, I. D.; Yamamoto, Y. *J. Am. Chem. Soc.* **2005**, *127*, 9844. (c) Nishikata, T.; Yamamoto, Y.; Gridnev, I. D.; Miyaura, N. *Organometallics* **2005**, *25*, 5025. (d) Gridnev, I. D.; del Rosario, M. K. C.; Zhanpeisov, N. U. *J. Phys. Chem. B* **2005**, *109*, 12498. (e) Patil, N. T.; Lutete, L. M.; Wu, H.; Pahadi, N.; Gridnev, I. D.; Yamamoto, Y. *J. Org. Chem.* **2006**, *71*, 4270. (f) Gridnev, I. D.; Kikuchi, S.; Touchy, A. S.; Kadota, I.; Yamamoto, Y. *J. Org. Chem.* **2007**, 72, 8371.

(46) (a) Bittner, M.; Koppel, H. *J. Phys. Chem. A* **2004**, *108*, 11116. (b) McKee, M. L.; Swart, M. *Inorg. Chem.* **2005**, *44*, 6975. (c) Kondo, T.; Tsunawaki, F.; Ura, Y.; Sadaoka, K.; Iwasa, T.; Wada, K.; Mitsudo, T. *Organometallics* **2005**, *24*, 905. (d) Nowroozi-Isfahani, T.; Musaev, D. G.; McDonald, F. E.; Morokuma, K. *Organometallics* **2005**, *24*, 2921.